JOURNAL OF GEOPHYSICAL RESEARCH, VOL. 102, NO. D8, PAGES 9335–9350, APRIL 27, 1997

Cloud simulations with the Max Planck Institute for Meteorology general circulation model ECHAM4 and comparison with observations

C.-T. Chen

Department of Earth Sciences, National Taiwan Normal University
Taipei

Erich Roeckner

Max Planck Institute for Meteorology, Hamburg, Germany

Abstract. In this study, cloud parameters as simulated by the latest version of the Max Planck Institute for Meteorology general circulation model are documented and compared with observations. The model simulations generally agree with the observed spatial distribution and temporal variation of the total cloud amount. There are, however, biases in the details. Underestimation in the total cloud amount found over the midlatitude oceans in summer leads to significant biases in the simulated radiation budget. Considerable uncertainties of the observed total cloud amount in the polar region call for improved measurement techniques for further model validation. With a similar mean state of total cloud amount in the tropics between model and observation, fewer daily and interannual variabilities are found in the model. Despite large uncertainties in the current cloud liquid water path retrievals, the main pattern and magnitude of the space-time distribution of cloud liquid water path is reseasonably well reproduced by the model. Lack of contrast between simulated cloud liquid water path in the subtropics and midlatitudes and failure to capture the observed summer local maxima of cloud liquid water path in the subtropical eastern ocean basins are the major discrepancies found in the model in comparison with the observations. The systematic differences in the magnitude of cloud liquid water path retrievals as shown in the comparison reveal a need for careful calibration of satellite retrieval algorithms. With a simple approach to prescribing land-sea contrast in cloud droplet number concentrations the simulated distribution of effective radii of cloud water droplets in the tropics is in good agreement with observations. However, some physical processes (e.g., precipitation efficiency and air mass advection) in regulating cloud droplet number concentrations cannot be resolved by the simple prescription. The model simulation of cloud effective drop radii over the midlatitude oceans reveals errors larger than those in other regions of the globe.

1. Introduction

It is recognized [e.g., *Intergovernmental Panel on Climate Control*, 1992] that the lack of understanding of clouds represents one of the largest uncertainties in climate modeling and prediction [*Cess et al.*, 1990; *Gates*, 1992]. Clouds exert a major impact on the Earth's radiation budget and hydrological cycle. But their spatial scales are normally too small to be resolved by climate models. Various parameterizations have been developed to represent clouds and their effects in climate models. The use of prognostic cloud water/ice equations in conjunction with cloud microphysical processes has also been explored [*Sundquist*, 1978; *Smith*, 1990; *Fowler et al.*, 1996]. However, these different considerations in cloud processes and their relation to large-scale variables are still one of the major sources of differences among the model results [*Cess et al.*, 1990]. Furthermore, observations validating cloud parameterizations and cloud microphysical properties are still limited. The complexity of cloud macroscale and microscale phenomena in different climate regimes and the limitation of spatial and temporal coverage from field experiments make the task difficult. The relationship between cloud parameters and the dynamic and thermodynamic states of atmosphere remains unclear. An additional problem that needs to be addressed is the different time-space scale used in in situ observation and modeling. Although satellite observation provides another valuable source of information on clouds, considerable deviations among different data sets and retrieval algorithms exist.

The direct influences of cloud macroscale and microscale parameters on cloud radiative effect and related hydrologic processes show the necessity of considering the essential cloud parameters in order to provide the physical link between the energy and hydrological cycle in the climate system. In addition to feedback processes resulting from changes in cloud macroscale quantities (e.g. amount, height), the potential cloud optical depth feedback mechanism as proposed by earlier studies [e.g., *Twomey*, 1977; *Somerville and Remer*, 1984; *Roeckner et al.*, 1987; *Liou and Ou*, 1989; *Charlson et al.*, 1992; *Albrecht*, 1989] emphasize the possible role played by cloud microphysical properties in affecting climate sensitivity. The consider-

Paper number 96JD03718.
0148-0227/97/96JD-03718$09.00

ation of differences in continental and maritime cloud microphysical properties also shows significant impact on the current climate simulation [*Kiehl*, 1994]. As a first step in illustrating the possibility of representing these physical processes and links in the atmospheric general circulation model (GCM), parameterization of cloud formation, formulation of sources and sinks in the cloud water transformation and bulk representation of cloud drop size based on the prognostic cloud water are incorporated into the fourth-generation atmospheric GCM developed at the Max Planck Institute for Meteorology in Hamburg (ECHAM4). This study documents and evaluates the cloud parameters simulated by ECHAM4. The effect of cloud on the simulated radiation budget in ECHAM4 has been discussed by *Chen and Roeckner* [1996]. Here we focus more on the cloud parameters themselves.

In the face of the difficulty in validating the cloud parameters generated by the model, we try to use various available sources of observational data to evaluate the simulated cloud parameters. We consider mainly the following parameters: total cloud amount, total cloud liquid water path, and the effective droplet radius in water cloud. Although different cloud types have been categorized in the satellite and ground-based cloud climatologies, both observations cannot reveal the three-dimensional picture because of cloud obscuration from the viewpoint. Additional data processing from the model output has to be performed before the comparison can be done. We did not attempt to do that here. The total liquid water path retrieval from the special sensor microwave imager (SSM/I) data [e.g., *Greenwald et al.*, 1993; *Weng and Grody*, 1994] provides near-global coverage of cloud liquid water path information to evaluate the model result. There is also a near-global survey of the effective droplet radii in water cloud derived from the International Satellite Cloud Climatology Project (ISCCP) data [*Han et al.*, 1994]. In the validation work we frequently show more than one observational data set. The purpose is to provide an estimation of the current range of cloud parameter retrieving techniques in addition to the uncertainty and error analyses in each data set as described in the respective documentation. In particular, for the total cloud liquid path, no ground truth is available to calibrate the satellite retrieval. The results from different retrieval algorithms sometimes do not even agree qualitatively.

The outline of this paper is as follows. Section 2 briefly describes ECHAM4 physical parameterizations particularly relevant to the simulation of cloud parameters, along with model results and the observational data sets used for the comparison. Sections 3 and 4 compare cloud cover and cloud microphysical properties, respectively, from the observations and ECHAM4 simulations. In addition to comparing global averages, zonal means, and geographical distributions of the available cloud parameters these sections also consider the seasonal cycle and temporal variation of the cloud parameters. Section 5 summarizes the findings.

2. Data Sets

2.1. Model

A detailed description of the dynamical and physical structure and the simulated climatology of ECHAM4 is documented by E. Roeckner et al. (1996). A shorter version of the model description can be found in a related model study on the validation of the Earth's radiation budget in ECHAM4 [*Chen and Roeckner*, 1996]. Only the main characteristics of the model and the physical parameterizations related to cloud simulations used in the study are highlighted here.

The prognostic variables in ECHAM4 include vorticity, divergence, temperature, surface pressure, water vapor, and cloud water. The standard resolution of the model is T42 (approximately 2.8° by 2.8° in longitude and latitude) with 19 hybrid vertical levels (top at 10 hPa). A semi-Langrangian transport method is used for the advection of moisture and cloud water [*Williamson and Rasch*, 1989]. Both annual and diurnal cycles are included in the model integration.

The mass flux scheme for deep, shallow, and mid-level convection [*Tiedtke*, 1989] has been modified with respect to the closure for penetrative convection and formulation of organized entrainment and detrainment [*Nordeng*, 1994]. Cumulus clouds are represented by a bulk model including the effect of entrainment (organized and turbulent) and detrainment (mostly through organized outflow at cloud top) on the updraft and downdraft convective mass fluxes. The detrained fraction of the convectively generated cloud water is coupled with the stratiform (anvil) cloud water equation. Shallow and mid-level convection depend on surface evaporation and large-scale vertical velocity, respectively.

The prediction of stratiform clouds is based on the cloud water transport equation including sources and sinks due to condensation/evaporation, as well as precipitation formation by coalescence of cloud droplets and sedimentation of ice crystals [*Sundquist*, 1978; *Roeckner et al.*, 1991]. Evaporation of cloud water and precipitation is considered. Sub-grid scale condensation and cloud formation are taken into account by specifying height-dependent thresholds of relative humidity [*Xu and Krueger*, 1991; *Walcek*, 1994]. Fractional cloud cover (b) is a nonlinear function of relative humidity [*Sundquist et al.*, 1989],

$$b = 1 - \sqrt{\frac{1 - r}{1 - r_0}} \tag{1}$$

where r is grid mean relative humidity and r_0 is the threshold value for condensation. The prescribed r_0 decreased linearly from the surface layer ($r_0 = 0.99$) to the top of the planetary boundary layer ($r_0 = 0.6$) and remains constant above the planetary boundary layer. The maximum cloud overlap assumption is used for contiguous cloud layers. Otherwise, random overlap is assumed. The liquid, ice, and mixed-phase clouds are diagnosed according to ambient temperature [*Matveev*, 1984; *Roeckner et al.*, 1991]. The effective radii of cloud droplets are parameterized from cloud water content. The number concentration of cloud droplets is specified (100 and 220 cm^{-3} are assigned to the low-level maritime and continental clouds, respectively, and gradually reduced to 50 cm^{-3} in the upper layers). A spherical shape is assumed for all liquid cloud droplets. The effective radii of ice crystal are functions of the ice water content based on empirical data [*Heymsfield*, 1977; *McFarlane et al.*, 1992].

The model simulated results are obtained from a 15-year integration with monthly observed sea surface temperature (SST) and sea ice for the period 1979–1993 extended from the so-called Atmospheric Model Intercomparison Project (AMIP) data set [*Gates*, 1992]. The model data reported are the ensemble annual and monthly means derived from the 15-year integration unless mentioned elsewhere.

2.2. Observations

International Satellite Cloud Climatology Project (ISCCP). A detailed description of the ISCCP data processing and products is given by *Rossow and Schiffer* [1991]. The analyzed visible and thermal infrared radiances from the NOAA Polar Orbiting Satellites and GOES, GMS, and METEOSAT Geostationary Satellites are first sampled at 30 km and 3-hourly resolution and normalized in calibration by reference to the NOAA 7 advanced very high resolution radiometer (AVHRR) to form the ISCCP-B3 data. Then these data are merged at 280 km resolution to become the ISCCP-C1 data. The C1 data products are then used to create the monthly statistics and resulting C2 data product. Calibration and adjustment procedures are used in various stages to improve the quality of the monitoring. The uncertainty of the cloud detection scheme is judged to be about 10–15% [*Rossow and Lacis*, 1990]. To evaluate the spatial and seasonal variation of the total cloud amount, the ISCCP C2 monthly mean cloud data product is used. The ensemble monthly average from available data between 1983 and 1990 are used for the comparison. To evaluate more detailed temporal variation, the daily mean of C1 product is used.

Another cloud parameter derived from ISCCP data is the effective drop radii in liquid water clouds [*Han et al.*, 1994]. The retrieval scheme, based on a radiative transfer model, relies on the ISCCP cloud detection and combines the cloud optical depth, cloud top temperature, surface reflectance, and surface temperature determined by ISCCP with 3.7 and 11 μm radiance from AVHRR measurement and the radiative transfer model to retrieve cloud particle size in water clouds (cloud top temperature of >273 K). The uncertainties in the results due to random error, calibration bias, inhomogeneity of clouds, and cirrus/aerosol contamination are normally less than 10%. It is not straightforward to compare the model results with the retrieved effective droplet radii in water cloud. While satellite data represent the effective drop radius required to produce the AVHRR channel 3 radiance with other input data from ISCCP, model-produced effective cloud drop radii are available in every layer where cloud water exists. To compare the effective drop radius, we select a fixed model layer where the water (low) cloud amount is largest among the different layers within ISCCP low cloud range (>680 mbar).

Ground-based cloudiness data. The data sources for this ground-based cloud observation are synoptic weather reports from land stations and ships' reports over the globe for the 10-year period from December 1981 to November 1991 [*Hahn et al.*, 1994] (hereinafter SFCC). Only the total cloud cover data are used for the comparison. The global observations are provided in 5° by 5° grid boxes. An analysis scheme is included in the data processing in order to reduce a night detection bias in previous cloud data archives from 1930 to 1980 [*Warren et al.*, 1986, 1988].

Special sensor microwave imager (SSM/I). The SSM/I is a passive remote sensing radiometer that measures the upwelling radiation in four spectral channels: 19.235, 22.235, 37, and 85.5 GHz. All frequencies are received in both horizontal and vertical polarization except the 22 GHz channel, which only measures in vertical polarization. Total liquid water path retrieval using the SSM/I data from the Defense Meteorological Satellite Program (DMSP) has been investigated recently [e.g., *Greenwald et al.*, 1993; *Liu and Curry*, 1993; *Weng and Grody*, 1994; *Karstens et al.*, 1994]. However, the published results of these workers do not agree. Total cloud liquid water path retrieval from microwave radiance can be affected by many input factors (e.g., total precipitable water, cloud temperature, surface wind, and sea surface temperature). There are also possible particle contributions from precipitation-size droplets in the retrieved cloud liquid water path. Currently, no ground truth for cloud liquid water path is available. Therefore, we use different data sets as an estimate of possible range for cloud liquid water path. Because of diffraction effects the spatial resolution of the measurements increases with frequency from a nadir footprint of 43 km at 19.35 GHz to 13 km at 85.5 GHz. For comparison the retrievals from microwave observations are spatially averaged to a 2.5° by 2.5° grid. Data are available only over ocean because of the variable microwave surface emissivity of land.

Table 1. Global and Hemispheric Mean Total Cloud Cover From ECHAM4 and ISCCP and *Hahn et al.* [1994] (SFCC) for Annual, January, and July Average

	Total Cloud Cover, %		
	Annual	January	July
ECHAM4			
G	59.9	62.3	58.5
NH	59.8	61.9	58.5
SH	60.0	62.7	58.6
ISCCP			
G	62.2	61.9	62.3
NH	58.8	57.2	61.4
SH	65.6	66.5	63.3
SFCC			
G	63.7	62.3	61.7
NH	61.8	60.8	63.9
SH	65.9	64.9	57.6

G, global mean. NH, northern hemispheric mean. SH, southern hemispheric mean.

3. Total Cloud Cover

3.1. Global Mean

The ensemble annually averaged global and hemispheric mean total cloud amounts (TCA) generated by the model, ISCCP, and SFCC are listed in Table 1. The missing data in the observation are not part of the averaging process. This approach may raise some concerns with regard to the SFCC data, since large areas in the southern hemisphere oceanic region are void of data. However, if we apply the area mask where data are available from SFCC to the ISCCP and model data, the major findings discussed later are not changed significantly. The annually and globally averaged TCA is slightly smaller in ECHAM4 than in both ISCCP and SFCC. While more annual mean TCA is found in the southern hemisphere in both observational data sets, the annual mean TCA in northern and southern hemispheres in ECHAM4 is almost the same.

The same quantities for January and July ensemble averages from ECHAM4, ISCCP, and SFCC are also listed in Table 1. There is good agreement between simulated and observed global mean TCA in January, while the simulated TCA in July is less than two observational data sets. Model simulation and observations show that January mean TCA in the southern hemisphere is larger than that in the northern hemisphere. However, the contrast is larger in ISCCP and SFCC. In July there is no difference in the two hemispheric mean TCA in ECHAM4. The two observational data sets, on the other hand,

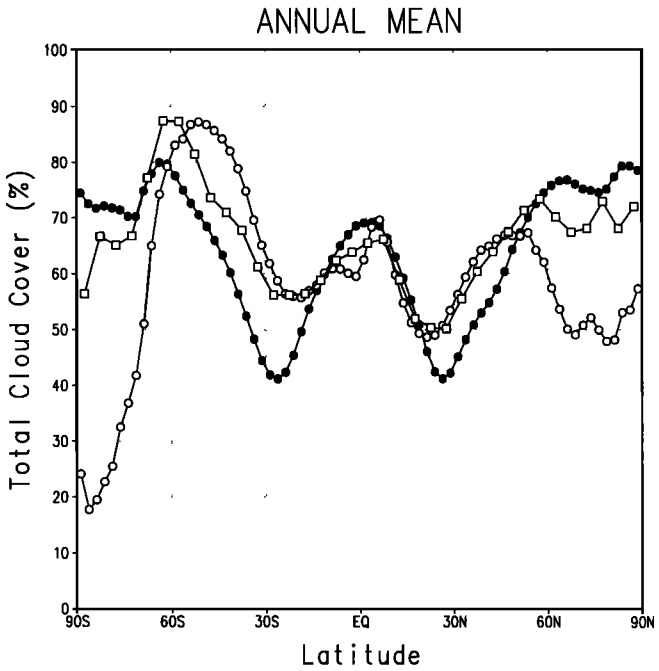

Figure 1. Annual and zonally ensemble averaged total cloud amount form ECHAM4 (solid circles), ISCCP (open circles), and SFCC (open squares).

show a contrast in TCA between the two hemispheres. For the hemispheric mean TCA, both observational data sets show a larger value in summer. The simulated TCA in both hemispheres is consistently greater in January.

3.2. Zonal Mean and Seasonal Cycle

The ensemble annually averaged zonal mean TCA in the three data sets is shown in Figure 1. Qualitatively, the latitudinal structure of TCA in the data sets is similar between 50°S and 50°N. Larger TCA is found in the tropical convergence zones and over the midlatitude storm track regions. The smaller TCA in the subtropics is related to the large-scale circulation pattern. While the simulated TCA in the tropics is in good agreement with both observations, there are systematic underestimates for the zonal mean TCA over the subtropics and midlatitudes in the model. Two observational data do not agree with each other in the high latitudes. The ground-based cloud climatology is always greater than the satellite-based one in the polar region. The TCA simulated by ECHAM4 in the northern hemisphere high latitudes is comparable to the SFCC. The simulated TCA over Antarctica is larger than the observed one.

To further illustrate the seasonal cycle of zonal mean TCA, the deviations of the zonally averaged monthly mean TCA from the respective annual mean value have been analyzed for ISCCP, SFCC, and ECHAM4 data. The amplitude and phase of the seasonal cycle of zonal mean TCA provide additional tests for validating the cloud simulation. Figures 2a–2c show the latitude-month distribution of the seasonal variation in zonal mean TCA from ECHAM4, ISCCP, and SFCC, respectively. Positive seasonal deviations of simulated TCA in the tropics are found mainly in the summer hemisphere. A similar seasonal cycle of tropical TCA is represented in ISCCP data, although the maximum of variation is closer to the equator in comparison with that of the model simulation. In addition, ISCCP has a larger amplitude in the northern hemisphere than ECHAM4, while the opposite holds for the southern hemisphere. The seasonal variation of zonal mean TCA in the tropics and northern hemisphere equatorward of 45°N in SFCC has a 1-month lag in comparison with the other two data sets. In ECHAM4, despite an agreement with ISCCP between 30°N and 45°N, the phase of seasonal variation near 60°N is opposite that in ISCCP. There is a wintertime increase of midlatitude TCA in the model. In the southern hemisphere midlatitudes, generally less than 5% amplitudes of the seasonal cycle are found in both model and observations throughout the year. There is no general agreement in the seasonal variation

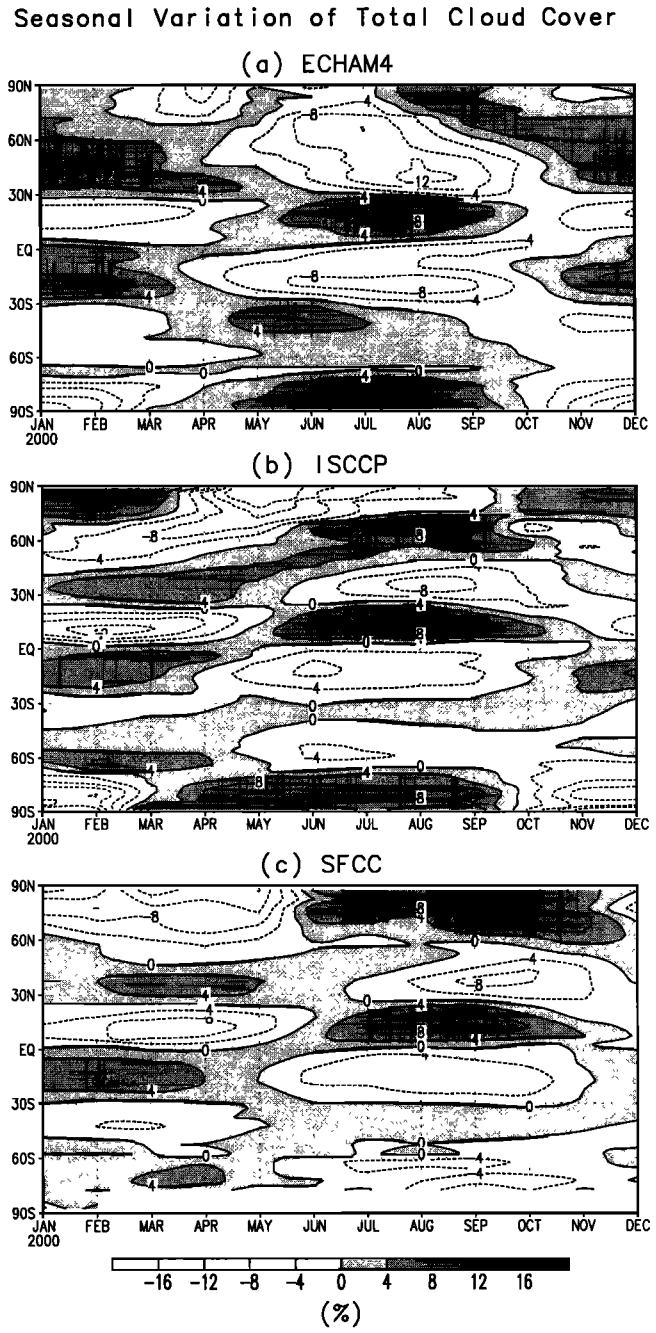

Figure 2. Latitude-month distribution of the seasonal variation in total cloud amount for (a) ECHAM4, (b) ISCCP, and (c) SFCC.

in zonal mean TCA over the polar regions. Similarity in the TCA seasonal variation over Antarctica is found between ISCCP and ECHAM4. But note that the annual mean TCA difference between ISCCP and ECHAM4 in the same region is about 50%. It emphasizes again the necessity to use both mean state and variability to validate the model cloud simulation. It is unlikely that the cloud feedback processes can be correctly captured if the seasonal change of cloudiness is unrealistic in the model. Also the large difference in the observed TCA over the polar regions in ISCCP and SFCC shows a need for improving the cloud retrievals in these areas. Our understanding of polar cloud systems is still very poor.

3.3. Geographic Distribution

Figures 3a–3c show the geographical distributions of ensemble January mean TCA from ECHAM4, ISCCP, and SFCC, respectively. Note that very few data over the southern hemisphere and oceanic region are available from the surface observations. Nevertheless, the TCA pattern of ISCCP and SFCC agree reasonably well, except over Europe, Russia, and Alaska, where larger TCA is found in SFCC. ECHAM4 reproduced the main pattern of the TCA distribution rather well. Major discrepancies are the underestimate over the midlatitude oceanic regions and overestimate over the northern hemisphere midlatitude continent. The overestimate is less significant when the model simulation is compared with surface observations. The amount of marine stratocumulus over the subtropical eastern Pacific in ECHAM4 is smaller than the observed amount. The extent of the simulated maximum TCA (more than 80%) over the Pacific warm pool, ITCZ, and SPCZ is broader than that in ISCCP. Considerable overestimates are also found over the Arctic and Antarctic regions in ECHAM4. However, as noted above, the quality of satellite and surface observations is degraded by the problems in the cloud identification over polar regions and the limited number of surface observations, respectively.

Geographical distributions of ensemble July mean TCA from ECHAM4, ISCCP, and SFCC are show in Figures 4a–4c, respectively. The large-scale pattern of TCA distribution between ISCCP and SFCC is again very similar. The main difference is over the Arctic region with larger values in SFCC. Similar to January, ECHAM4 underestimates TCA over the midlatitude oceanic region. These underestimations in TCA in the model lead to the underpredicted shortwave cloud radiative forcing found over the region [*Chen and Roeckner*, 1996]. TCA simulations over the continents agree well with ISCCP except for the underestimate of cloud amount over the western United States. Subtropical cloudiness over the ocean is also generally underestimated in the model. Although a fair amount of marine stratocumulus is simulated off the west coast of continents in the subtropics, it is not extended far enough over the ocean, as indicated in the observations. The overestimated TCA in the West Pacific warm pool region is indicative of enhanced water vapor transport in convectively active regions. The excessive large-scale subsidence in the equatorial eastern Pacific [*Chen et al.*, 1996] leads to a slight decrease in TCA over the Intertropical Convergence Zone (ITCZ) between 110°W and 150°W in comparison with the relatively uniform TCA along the ITCZ in ISCCP data.

3.4. Temporal Variation

A diurnal cycle in the cloud cover has been shown to exist in the ISCCP data [*Rossow*, 1993] and other studies [e.g., *Minnis and Harrison*, 1984; *Wylie et al.*, 1994]. A systematic diurnal variation in cloudiness not only affects the variation of the radiation budget and therefore possible interactions with other fields, but also influences surface processes by altering the radiative part of the surface energy budget. The diurnal cycle is included in the ECHAM4 integration. This section provides

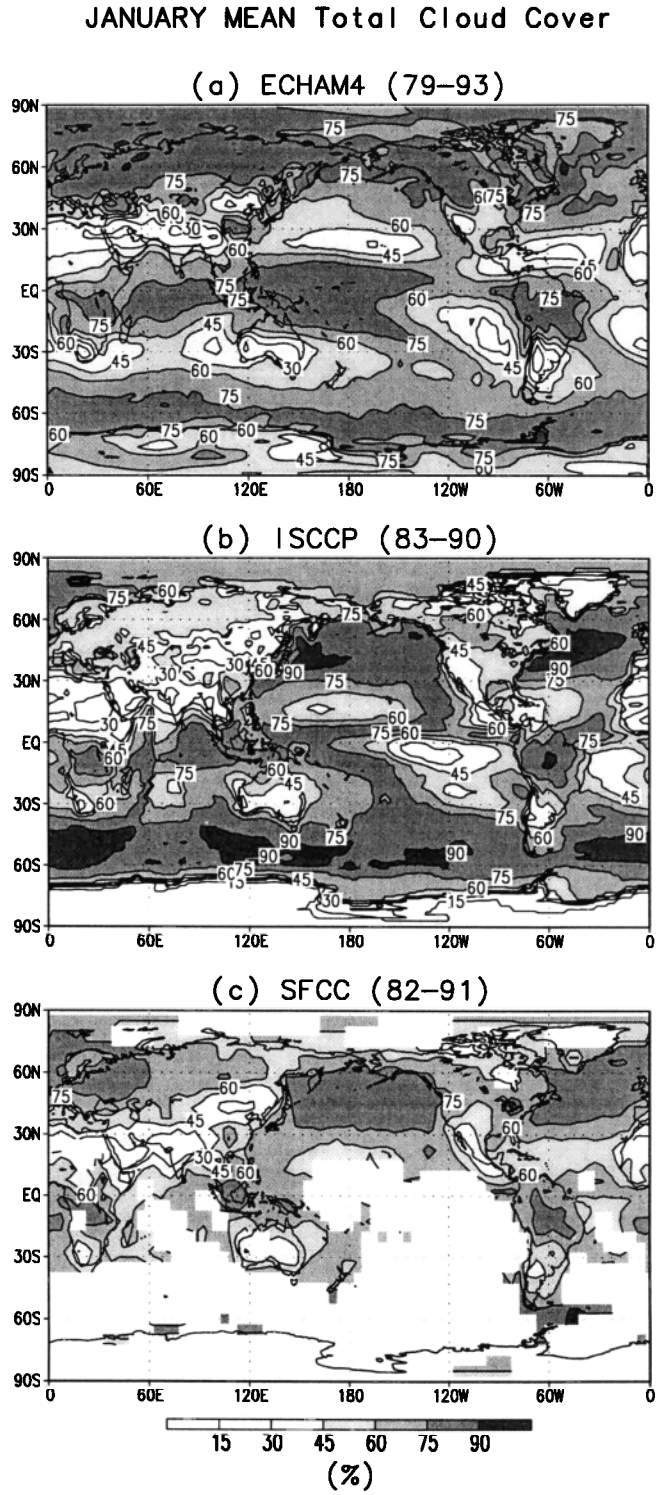

Figure 3. Geographic distribution of the ensemble January mean total cloud amount for (a) ECHAM4, 1979–1993; (b) ISCCP, 1983–1990; and (c) SFCC, 1982–1991.

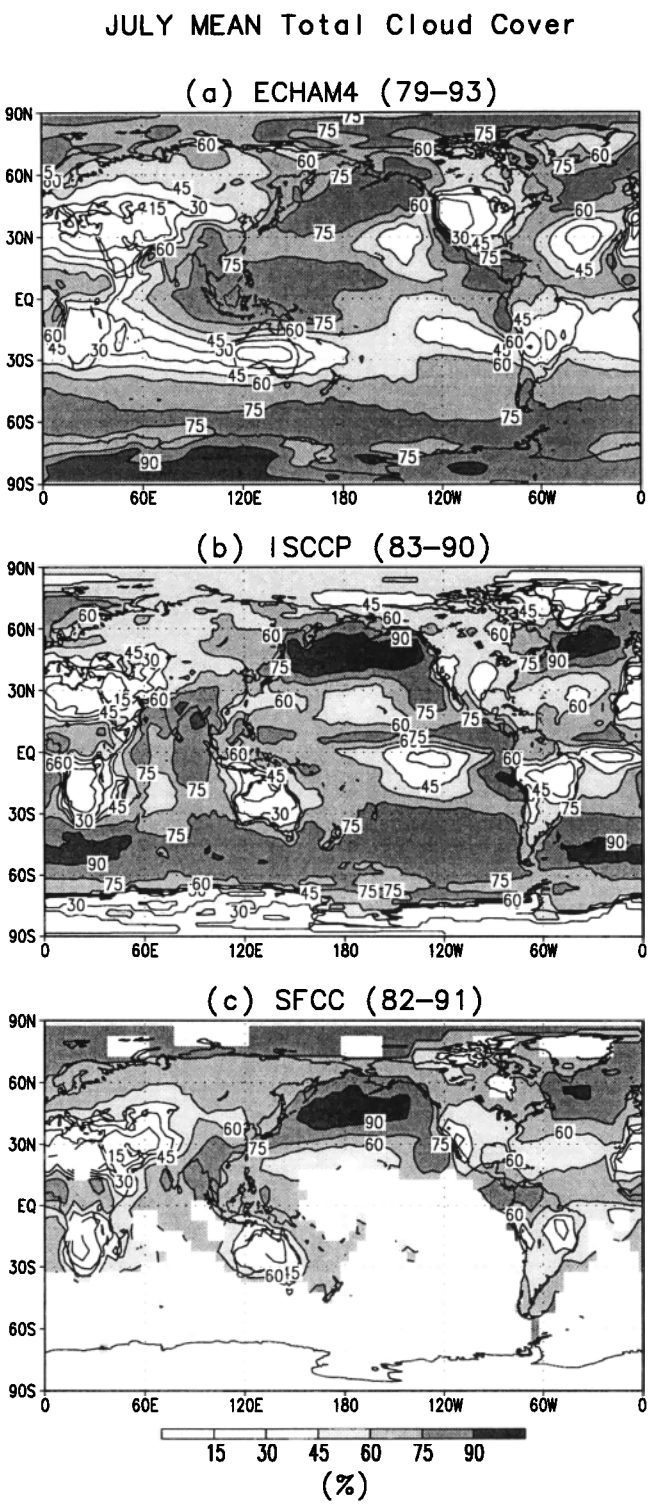

Figure 4. As in Figure 3 except for July.

a good opportunity to examine the model's ability in producing the diurnal variation of cloudiness.

Table 2 shows the area-averaged TCA at local time as simulated by the model and observed by the ISCCP for January 1989. Since the model history output is a 6-hourly mean value, the area averages at local time are divided into four intervals, 0000–0600, 0600–1200, 1200–1800, and 1800–2400. The ISCCP C2 monthly mean data contain TCA information with 3-hourly temporal sampling. Area-averaged TCA are placed in eight local time bins (from 0000 to 2100). Note that these fixed local hour bins are used to represent the closest local time for the chosen regions. Although, in the model, the number of intervals in a day is rather limited, it keeps the minimum amount of information required to reveal the diurnal cycle.

Over the eastern United States (EUS), an area between 90°W-75°W and 30°N-45°N), ISCCP data show an afternoon maximum TCA. There is a similar tendency in the model simulation, except that the magnitude of diurnal variation in TCA is smaller. The large surface temperature variation over land area is expected to affect the local evaporation and the development of the afternoon cloudiness maximum. Over the equatorial Pacific (EP), between 150°E-165°E and 10°S-10°N) and the northern Pacific (NP), between 150°E-165°E and 40°N-50°N), there is no clear diurnal TCA variation in either the ISCCP data or the model simulation. Over the southern subtropical Pacific (SSP), between 120°W-105°W and 20°S-5°S), a peak in TCA before dawn is found in ISCCP data. A similar maximum TCA in the morning is also well captured by the ECHAM4. The ocean with its large heat capacity does not have significant diurnal variations in the surface temperature. The formation of low-level cloud generally peaks in value before dawn in response to the diurnal change in boundary layer structure over the ocean [*Randall et al.*, 1984]. Over the Amazonian (AM) region, between 60°W-45°W and 20°S-5°S), the diurnal signal is mixed in ISCCP, while a peak TCA in the morning is simulated by ECHAM4.

Figures 5a and 5b show the standard deviation of daily mean TCA in January 1988 from ECHAM4 and ISCCP, respectively. Daily mean data averaged from the ISCCP C1 are used for the calculation. The main features in the observation (Figure 5b) are (1) relatively large variability in the tropics, highlighting the large total cloud change associated with tropical disturbances and convective events, (2) persistent large total cloud amount over the midlatitude oceanic areas, significantly reducing the day-to-day variability, and (3) generation by the midlatitude cyclonic cloud systems of considerable variability over the northern hemisphere continents. The daily standard deviation in the model reveals similar variability in the subtropics in comparison with the observations (Figure 5a). Over the ITCZ and convective centers the variability in the simulated TCA is considerably smaller than that in the ISCCP data. Consistently large daily mean TCA (>60%) found in the model greatly reduces the day-to-day variability for these tropical regions, especially in the upper troposphere, where large cloud amount is easy to form with abundant moisture advection from below. ECHAM4 can reproduce the relative minimum standard deviation of the daily mean TCA in the southern hemisphere midlatitudes, although the magnitude is still greater than that in ISCCP. Larger TCA variability is predicted by the model over the northern hemisphere midlatitude oceanic regions than that in ISCCP. Over these storm track regions, ISCCP reveals a sharp increase in TCA throughout the month in comparison with TCA over the adjacent continents. This persistent large daily mean cloud cover over oceanic region reduces the observed day-to-day variability. More TCA fluctuations in the model are associated with the passage of westward propagating cyclonic systems. On the contrary, over the continent at the same latitude these cyclonic cloud systems occasionally cause an increase of TCA in the ISCCP observations on a synoptic timescale, which results in a relatively large standard deviation in comparison with the oceanic regions.

Table 2. Area-Averaged Total Cloud Cover at Local Time From ECHAM4 and ISCCP for January 1989

Area	Local Time							
	0000	0300	0600	0900	1200	1500	1800	2100
ISCCP								
EUS (90°W-75°W, 30°N-45°N)	50	49	48	49	57	56	45	49
EP (150°E-165°E, 10°S-10°N)	81	80	79	74	78	80	82	81
NP (150°E-165°E, 40°N-50°N)	67	67	67	65	66	64	65	67
SSP (120°W-105°W, 20°S-5°S)	40	48	45	37	38	37	33	34
AM (60°W-45°W, 20°S-5°S)	80	84	82	79	81	78	77	79

	6-Hour Mean			
	0000–0600	0600–1200	1200–1800	1800–2400
ECHAM4				
EUS (90°W-75°W, 30°N-45°N)	51	52	56	53
EP (150°E-165°E, 10°S-10°N)	87	87	86	86
NP (150°E-165°E, 40°N-50°N)	62	61	58	60
SSP (120°W-105°W, 20°S-5°S)	35	39	25	25
AM (60°W-45°W, 20°S-5°S)	77	80	71	69

Values are in percent.

Consistently larger cloudiness is found in the model simulation from eastern Europe to Siberia and therefore less daily variability. Similar results are found in July (Figures 6a and 6b). The contrast in the daily TCA variability in the northern hemisphere midlatitudes oceans and continents is better reproduced. The persistent dryness and small TCA over the Mediterranean Sea, Arabian Peninsula, and northeastern Africa is simulated well in the model.

Figures 7a and 7b show the interannual standard deviation of the annual mean TCA from ECHAM4 and ISCCP, respectively, derived from data between 1984 and 1990. The deficiency in simulating the interannual variability of TCA in the tropics by ECHAM4 is noted by *Chen and Roeckner* [1996]. The standard deviation from the available observations is largest in the central equatorial Pacific, since the cloud distribution is strongly influenced by the large-scale circulation changes associated with El Niño-Southern Oscillation (ENSO) events (Figure 7b). The stronger tropical TCA variability in the model, however, is located near 120°E and 150°W (Figure 7a), different from that in ISCCP. In the model the TCA remains very large for most of the western equatorial Pacific. Therefore, although the region with large cloud amount indeed shifts when ENSO events occur, large interannual variations of annual mean TCA only show up around the edge of the large cloud amount area. It is also worthwhile to note that the pattern of the interannual variability in simulated total cloud water path, on the other hand, is closer to observed TCA interannual variability [*Chen and Roeckner*, 1996]. This finding raises a question on the parameterization of cloud cover in the model. A variety of formulations relate large-scale variables (mainly relative humidity) to the extent of cloud cover in the model empirically or on the basis of results from a cloud ensemble model. Cloud cover and cloud liquid water content are not directly related to each other in the model. One possible refinement of the current sub-grid scale cloud cover formation scheme is to include the information of the prognostic cloud water. Serious tests must be performed to evaluate these different parameterizations, not only for a good representation of the mean field, but also for the temporal variability. However, even for the mean cloud fields there are huge differences

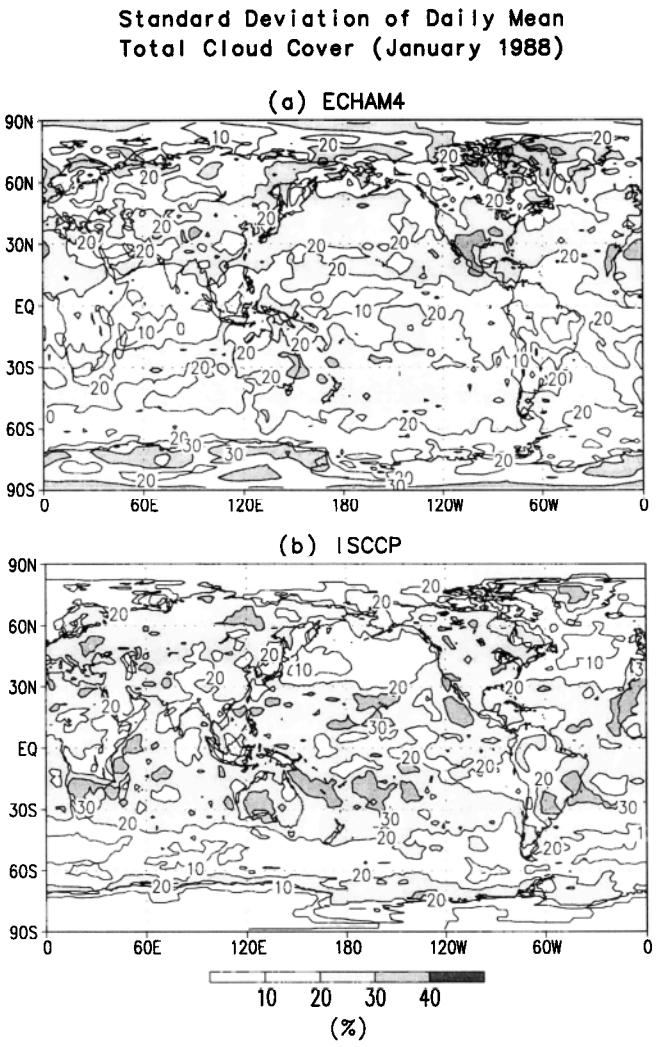

Figure 5. Geographic distribution of standard deviation of daily mean total cloud amount in January 1988 for (a) ECHAM4 and (b) ISCCP.

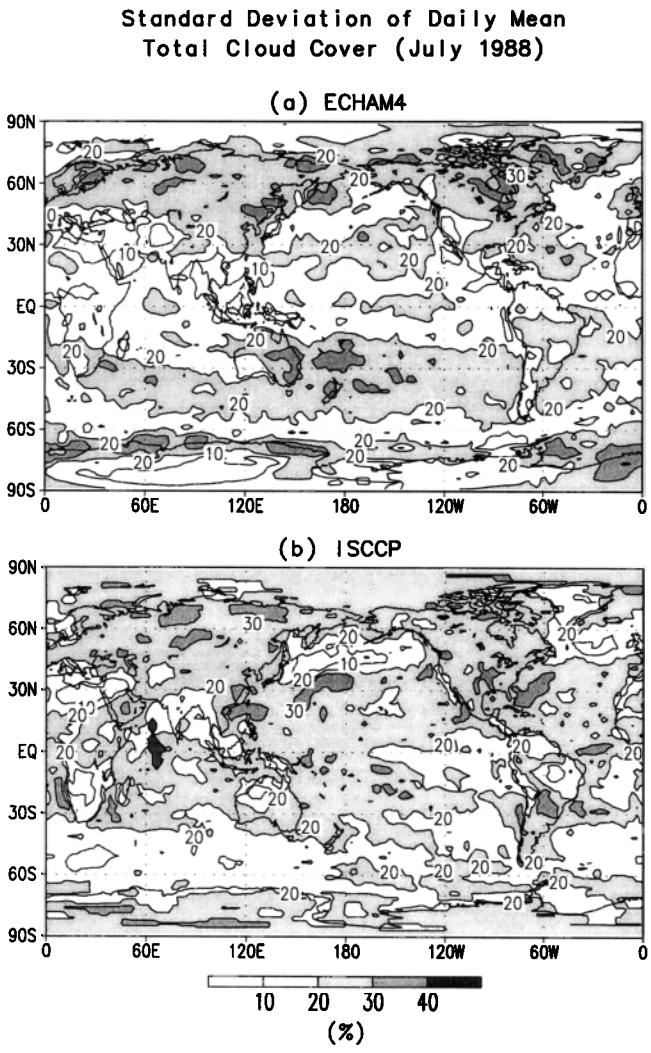

Figure 6. As in Figure 5 except for July.

among the climate models [*Weare et al.*, 1995]. Another related issue is the methodology for comparing the observed and simulated TCA. The assumption on cloud overlap and cloud emissivity in two types of data sets can significantly affect the outcome.

4. Total Cloud Liquid Water Path

SSM/I cloud liquid water retrievals are used to evaluate the model cloud water simulations. In view of the large differences among different retrieval techniques and the lack of ground truth, we select two retrieved data sets serving as an estimate of possible range. One should keep in mind that large uncertainties are involved in these observed data. However, it is currently one of the best techniques available to estimate near-global distribution of total cloud liquid water path (CLWP). On the other hand, the representation of cloud microphysical properties in the climate model is also in a primitive stage. ECHAM4 separates the prognostic water cloud into liquid and ice according to the ambient temperature. Although it is a crude empirical method, for a fair comparison we integrated the liquid part from the prognostic cloud water content to obtain the CLWP.

4.1. Global Mean

Because of the limitation of SSM/I data over land and sea ice the comparison is restricted to oceanic regions equatorward of 60°. The global, hemispheric, and zonal mean CLWP shown below is actually restricted to this domain. The ensemble annually averaged global and hemispheric mean total CLWP generated by the model and two SSM/I retrievals are listed in Table 3. Note that the difference in annually and globally averaged CLWP in two retrievals is nearly a factor of 2. The model's result shows an intermediate value between the two SSM/I retrievals. Both observed data sets show slightly more annual mean CLWP in the southern hemisphere, while there is more CLWP in the northern hemisphere in the model. All three data sets show a larger global and hemispheric mean CLWP in July in comparison with January.

4.2. Zonal Mean and Seasonal Cycle

The latitudinal structure of ensemble annual mean CLWP from the model and SSM/I retrievals is shown in Figure 8. Both SSM/I retrievals show a narrow local maximum near 5°N corresponding to the ITCZ. The higher CLWP found in midlati-

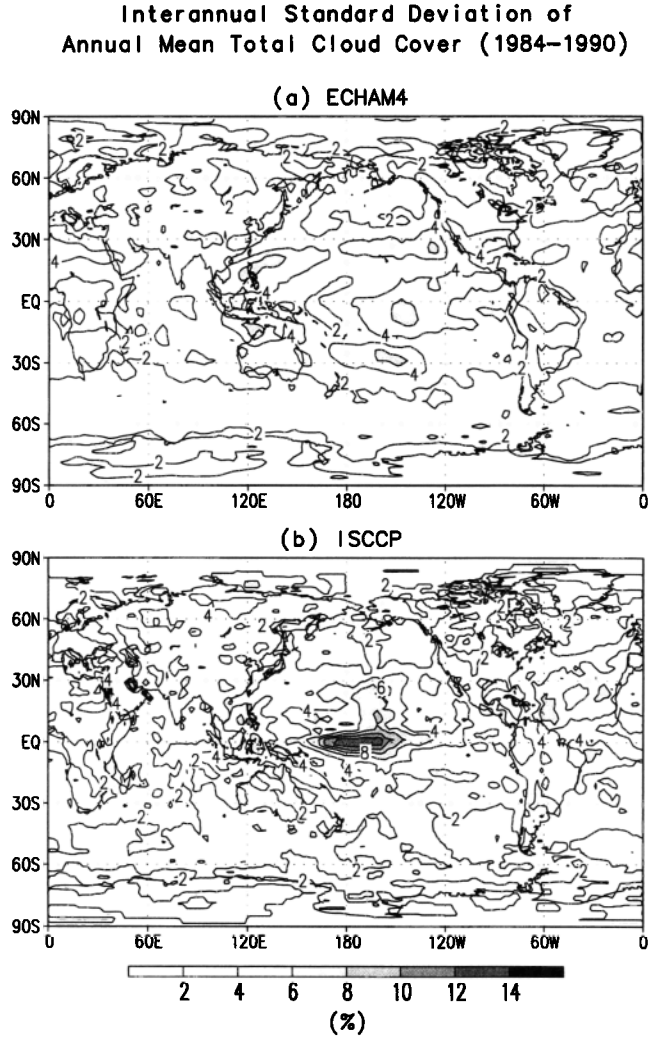

Figure 7. Geographical distribution of the interannual standard deviation of annual mean total cloud amount for (a) ECHAM4 and (b) ISCCP. Data from 1984–1990 are used to calculate the interannual standard deviation.

Table 3. Area Average Values of Total Cloud Liquid Water Path From ECHAM4 and SSM/I Retrievals for Annual, January, and July Average

	Total Cloud Liquid Water Path, g/m^2		
	Annual	January	July
ECHAM4			
G	70.5	70.7	72.6
NH	71.0	73.0	75.0
SH	70.1	68.9	70.9
SSM/I [*Greenwald et al.*, 1993]			
G	81.5	78.4	84.0
NH	80.3	81.2	82.0
SH	82.3	76.4	85.4
SSM/I [*Weng and Grody*, 1994]			
G	51.1	50.6	52.5
NH	48.1	49.8	51.0
SH	52.8	50.9	53.2

G, NH, and SH denote the area average of 60° equatorward over the ocean in both hemisphere, northern hemisphere, and southern hemisphere, respectively. Available data from 1987 to 1991 are used.

tudes in the two observed data coincide with the location of storm tracks and frequent low-cloud occurrence region [*Warren et al.*, 1988]. Large systematic differences (~30 g/m^2) in the two retrievals are found for almost all latitudes. This finding reiterates the current uncertainty about our knowledge on global cloud liquid water distribution. Near the tropical convergence zone the model predicts more CLWP than the retrieval from *Weng and Grody* [1994] (hereinafter WG94) indicates. However, it is close to the retrievals from *Greenwald et al.* [1993] (hereinafter G93). Note, however, that the retrieval in the tropics is one of the weaknesses in the latter data set as discussed by G93. Over the midlatitudes the model simulation is closer to that of WG94. Between 20° and 40° in both hemispheres the model simulation falls in between the results from two SSM/I data sets. Relatively low contrast in the annual mean CLWP between the subtropics and midlatitudes is found in the model. The major differences from G93 is the underpredicted CLWP in the summer oceanic midlatitudes, probably related to the underestimate of cloud amount and planetary albedo in the model [*Chen and Roeckner*, 1996]. On the other hand, the differences between WG94 and the model data are found mostly in the relatively dry subsidence region.

To further illustrate the simulation of the seasonal cycle of the zonal mean CLWP, the deviation of the zonally averaged monthly mean CLWP from the respective annual mean value has been analyzed for ECHAM4 and both SSM/I retrievals. Despite the large uncertainties from SSM/I CLWP retrievals, seasonal variations provide additional information for validating the model CLWP simulation. Figures 9a–9c show the latitude-month distribution of the seasonal variation in zonal mean CLWP from ECHAM4, G93, and WG94, respectively. In the tropics the seasonal cycle of simulated CLWP follows the seasonal migration of the ITCZ with larger CLWP value in the summer hemisphere. CLWP maxima are found in summer over the higher latitude and in winter over the subtropics in all three data sets, although there are differences in the details. In the previous discussion we found a similarity in the annually and zonally averaged CLWP near the ITCZ between G93 and ECHAM4; nevertheless, the large tropical seasonal variation found in the model is almost absent in the work of G93. G93 has a CLWP seasonal cycle in the southern hemisphere midlatitudes comparable to the model simulation and a slightly larger variation in the northern hemisphere midlatitudes. WG94, on the other hand, have a more clearly ITCZ induced CLWP variation in the tropics than does G93, although the magnitude of the variation is still less than ECHAM4. The larger-amplitude seasonal cycle in the tropical CLWP is the likely reason for the overestimation of the seasonal change in the shortwave cloud radiative forcing in the model [*Chen and Roeckner*, 1996]. Smaller variations in the southern hemisphere subtropics are found by WG94, while the opposite holds for the northern hemisphere subtropics. Good agreement between WG94 and the model can be found in the higher latitudes. It is worthwhile to note that the algorithm used to retrieve CLWP not only affects the mean quantity but also can exert considerable impact on the seasonal variation.

4.3. Geographic Distribution

Figures 10a–10c show the geographical distribution of ensemble January mean CLWP from ECHAM4, G93, and WG94, respectively. The main pattern of observed CLWP is well captured by the model, especially the location of the ITCZ and the storm tracks. Over the southern ocean the model simulation is closer to that of WG94. Considerably larger CLWP values in the southern ocean are shown by G93. While similar magnitudes of CLWP from ECHAM4 and G93 are found in the subtropics, lower subtropical CLWP is found by WG94. It should be emphasized that the comparison of the absolute CLWP values from the model and observations does not serve as a strict model validation. Because of the large uncertainty in the observation and crude separation of liquid and solid phase of cloud water in the model, we limit the scope to whether the reasonable range (from various retrieval algorithms) of CLWP and the main pattern in geographic distri-

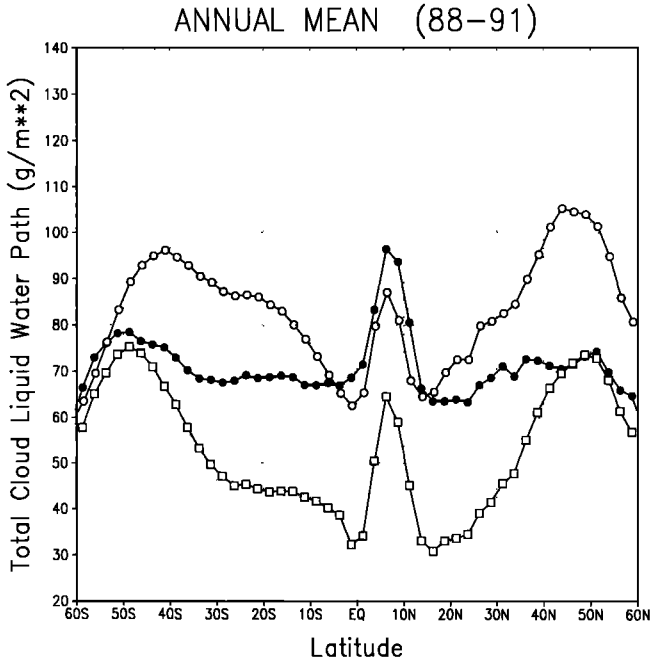

Figure 8. Annual and zonally ensemble averaged total cloud liquid water path amount from ECHAM4 (solid circles), SSM/I Greenwald's retrieval (open circles), and SSM/I Weng and Grody's retrieval (open squares).

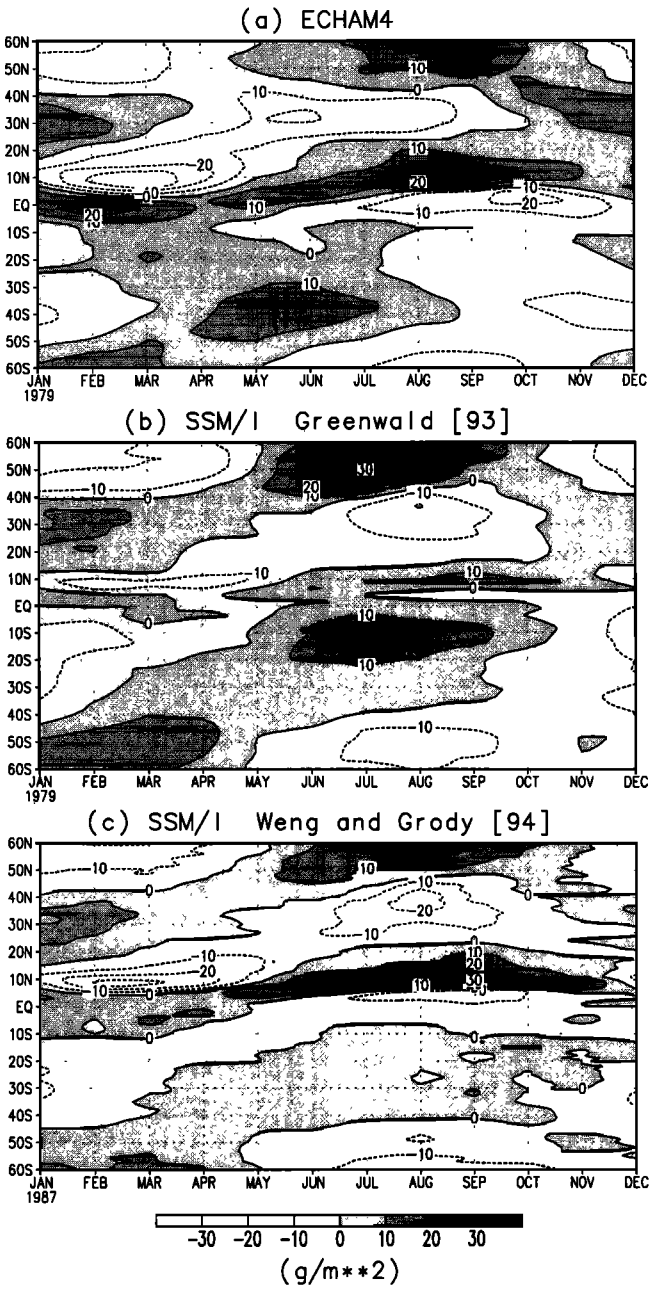

Figure 9. Latitude-month distribution of the seasonal variation in total cloud liquid water path for (a) ECHAM4, (b) SSM/I Greenwald's retrieval, and (c) SSM/I Weng and Grody's retrieval.

bution can be captured by the simple parameterization in the model.

The geographical distribution of ensemble July mean CLWP from ECHAM4, G93, and WG94 are shown in Figures 11a–11c, respectively. The main pattern of the observed local maximum CLWP associated with ITCZ and midlatitude circulation system is again predicted by the model. In addition, differences in CLWP between the model and the results of G93 over the midlatitude and between the model and the results of WG94 over the subtropics are similar to those shown in January results. One bias of the pattern in the model is over the subtropical eastern ocean basins. While the minima in CLWP are limited to near the coast in the SSM/I retrievals with a relatively large CLWP farther away from the coast corresponding to the prevalence of marine stratocumulus, the model actually has local minima opposite to the observations in these regions.

No direct measurements of the global distribution of ice water path are available at present. Although the separation of liquid and ice water in the model uses only a simple empirical function, it is worthwhile to show the ice water simulation for a more complete picture of the model result. It also serves as a first-order indication for the model result in simulating the vertical distribution of cloud water. Figures 12a and 12b show the ensemble average of simulated total cloud ice water path in January and July, respectively. The maxima in the tropics indicate the deep convection centers in the model. The large ice water path is produced within the deep convection centers over the equatorial oceans in January and the convection centers over central America, Congo River basin, and Indonesia with extension into the central Pacific along the ITCZ in July. The feature highlights the influence from the tropical circulation simulated in the model. Strong subsidence in the equatorial eastern Pacific and off the west coast of the continents in the

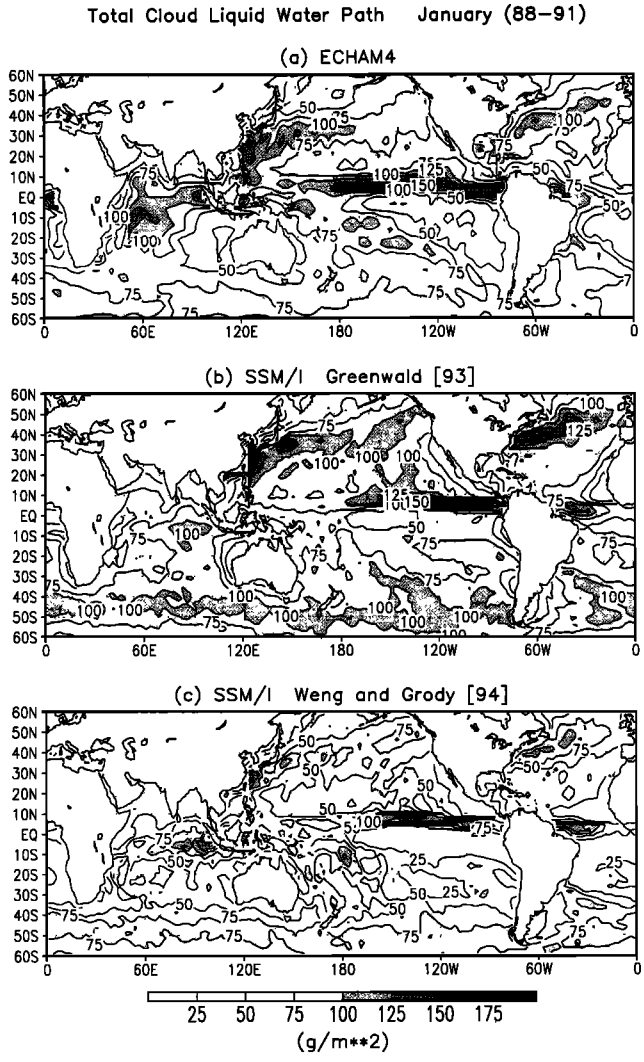

Figure 10. Geographic distribution of the ensemble January mean total cloud liquid water path from 1988 to 1991 for (a) ECHAM4, (b) SSM/I Greenwald's retrieval, and (c) SSM/I Weng and Grody's retrieval.

summer hemisphere significantly suppresses the ice water path. A relatively large ice water path is also found over the midlatitude ocean with more ice water in the winter hemisphere. This is expected from the seasonal atmospheric temperature change.

4.4. Temporal Variation

The tropical interannual variability of total cloud water path (both liquid and ice) in the model is found to be closely related to the well-simulated cloud radiative forcing anomalies [*Chen and Roeckner*, 1996]. Here we investigate whether the liquid part of the tropical total cloud water path anomalies has also been observed in the SSM/I data sets. Figures 13a–13c shows the tropical CLWP anomalies over the ocean (averaged between 5°N and 5°S) from ECHAM4, G93, and WG94, respectively. A 5-month running mean is applied to the monthly CLWP anomaly fields. Note that the data from G93 are available between July 1987 and December 1991, and the data from WG94 are available to the end of the model integration. The missing data between late 1990 and late 1991 of WG94 are due to the failure of the 85 GHz channel used in the retrieval algorithm. The anomalies in the model are clearly affected by the recent ENSO events, as is apparent from the shift in the active convective zone in the equatorial Pacific. Interestingly, quite different tropical interannual variability is found in the two SSM/I retrievals. The location and magnitude of anomalies in the work of WG94 is quite close to the model simulation, while very small tropical variation is observed by G93. The less reliable tropical result as discussed by G93 shows not only rather small seasonal variation but also less sensitivity to the SST change on an interannual timescale.

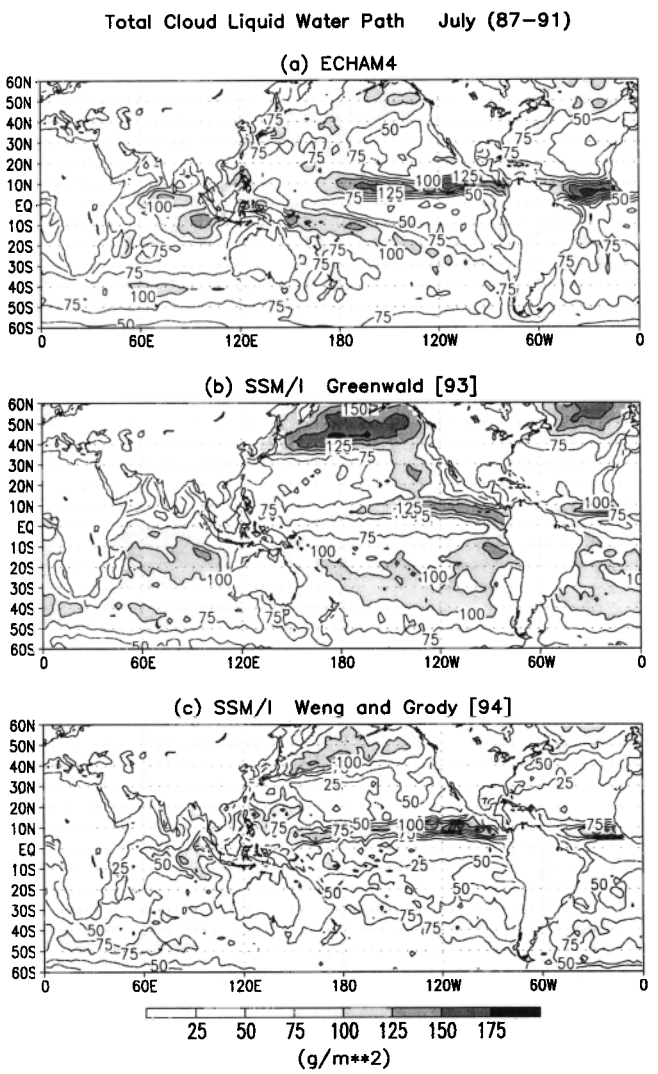

Figure 11. As in Figure 10 except for July.

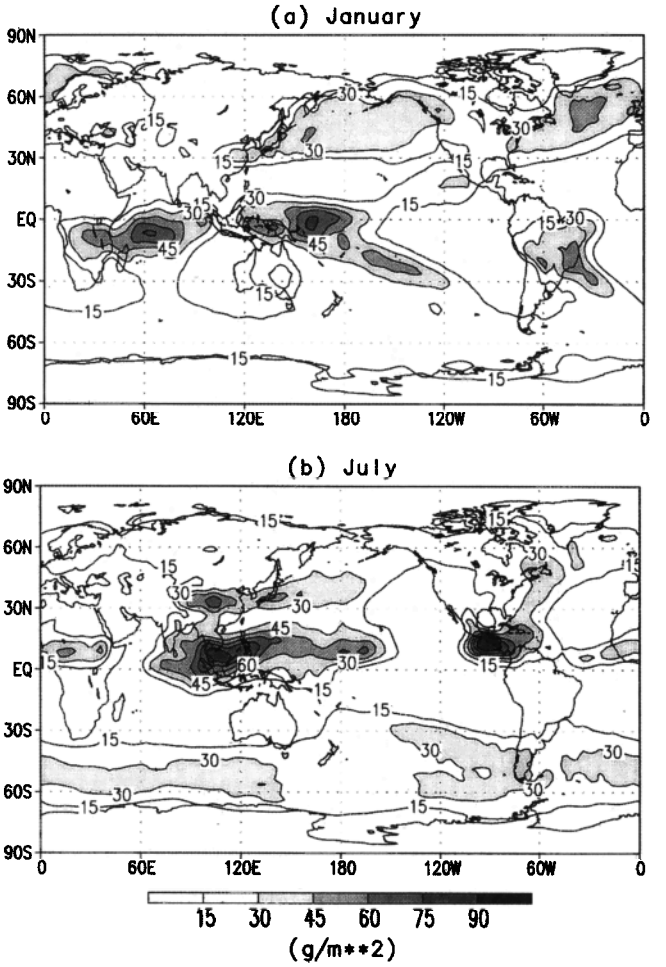

Figure 12. Geographic distribution of the ensemble mean total cloud ice water path from 1979 to 1993 as simulated by ECHAM4 for (a) January and (b) July.

Diurnal variation of CLWP has been shown by WG94. The observed morning maximum at 0530 local solar time over the ITCZ, the South Pacific Convergence Zone, and the North Pacific is consistent with other cloud analyses (WG94). Figure 14a is a Hovmöller diagram of the simulated CLWP at 16.25°N from April to September 1985. Diurnal variation of CLWP similar to that in the SSM/I data (WG94) is found in ECHAM4. The CLWP diurnal cycle in the tropics is evident not only in the propagating tropical disturbances but also in the more stationary local variations. The coherent structure and propagating speed of the major high-CLWP events are consistent with the finding by *Lau and Crane* [1995] using the cloud optical depth data from ISCCP. The diurnal cycle is also found in the simulated ice water path at the same latitude (Figure 14b). The location of a large ice water path is mainly associated

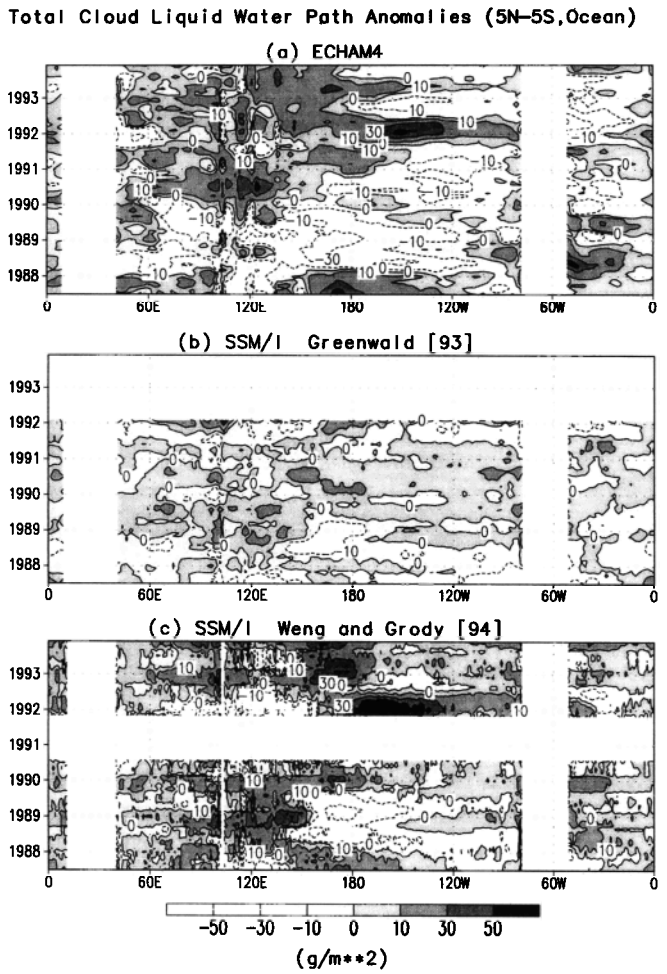

Figure 13. Longitude-time distribution of the equatorial (averaged 5°N-5°S) total cloud liquid water path anomalies over the ocean for (a) ECHAM4, (b) SSM/I Greenwald's retrieval, and (c) SSM/I Weng and Grody's retrieval. A 5-month running mean is applied.

with high CLWP and the occurrence of organized deep convective activities. Less diurnal variation is found for the cloud system associated with extratropical wintertime cyclonic systems as revealed in the Hovmöller diagram for CLWP from January to March 1985 at 46.25°N (Figure 15). Again the propagating speed and the coherence pattern of the simulated cloud systems correspond well with the midlatitude circulation systems shown in the study by *Lau and Crane* [1995]. The disruption of the coherent structure in northeast China and near the coast of the United States is also revealed in ISCCP cloud optical thickness data. A larger portion of total cloud water path at this latitude is in the ice phase and corresponds well to the high-CLWP events shown previously; i.e., the cloud systems simulated in this area mostly have considerable vertical extent.

4.5. Effective Radii for Liquid Water Cloud

A near-global survey of the effective drop radii in water cloud using ISCCP data by *Han et al.* [1994] (hereinafter H94) is used to assess the effective drop radius in water cloud predicted in the model, which assumes water droplets are spheres and prescribes the number concentration of cloud droplets separately for cloud formed over the land and ocean. An earlier study by *Boucher and Lohmann* [1995] used simulated fields of sulfate aerosol mass and the empirical relation between sulfate aerosol mass concentration and cloud droplet number concentration to assess the indirect effect of anthropogenic sulfate aerosols on climate. In their study the cloud effective drop radii simulated with a preliminary version of the ECHAM4 at T21 resolution was evaluated the H94 data. The land-sea contrast in the observation was reasonably produced. However, the zonal mean values in the ECHAM model are lower than observed data over both land and sea. Also note that the effective drop radii in water cloud derived from ISCCP and the referred study do not use the same procedure.

Here we did not attempt to do a similar exercise. Instead we choose a model layer representing the level with major low-level cloud cover and within the vertical domain where the land-sea contrast in the prescribed cloud drop number concentration is still effective. The level 15 (approximately 850 hPa) in the model's hybrid vertical coordinate is used for the following illustration. Areas with no liquid water are assigned as a missing point in the model results. The missing data in the observation are due to the domain limitation of H94 and the availability of the liquid water cloud (defined as cloud top temperature of >273 K). Figures 16a and 16b show the monthly mean effective cloud radii in July 1988 from ECHAM4 and H94, respectively. Strong land-sea contrast is found in most of the observational data except in the active convective centers over land and particularly in regions where monsoonal circulations dominate. This finding may be due to the frequent precipitation, which reduces the number of cloud condensation nuclei and also the strong ventilation of the boundary layer by convection associated with strong low-level advection from nearby oceans (H94). The land-sea contrast in cloud droplet number concentration in the model cannot include mechanisms such as the influence from the air mass advection across the coastline or reduced drop number concentration from the frequent precipitation area. However, the ECHAM4 model can still simulate reasonably well the magnitude of the water cloud effective radii and the land-sea contrast in the tropics. The model indeed predicts smaller drop radii off the west coast of the continents, although it is extended farther away from coast. The model result is due to the relatively small CLWP as simulated in the model (Figure 11a) and different from the influence of advection of continental air as suggested by H94. The larger effective radii in the convective region over land are absent in the model because of the limitation of the parameterization as indicated above. Other significant differences are found over the midlatitude oceans in the northern hemisphere. Relatively large cloud amounts simulated over the region considerably reduce the in-cloud cloud water content available to form cloud drops and therefore the drop size. However, such an influence from the frequency of cloud occurrence is not evident in the work of H94, although large cloud amounts over this region are also shown in the observations (Figure 4b). The comparison reveals the shortcoming of the model parameterization and points to the direction for further improvement. But recall that the definition of effective radii for water cloud is not exactly the same in the model and the observations, respectively. The methodology for comparison of cloud effective radii inferred from observation and simulated in the model also deserves further investigation.

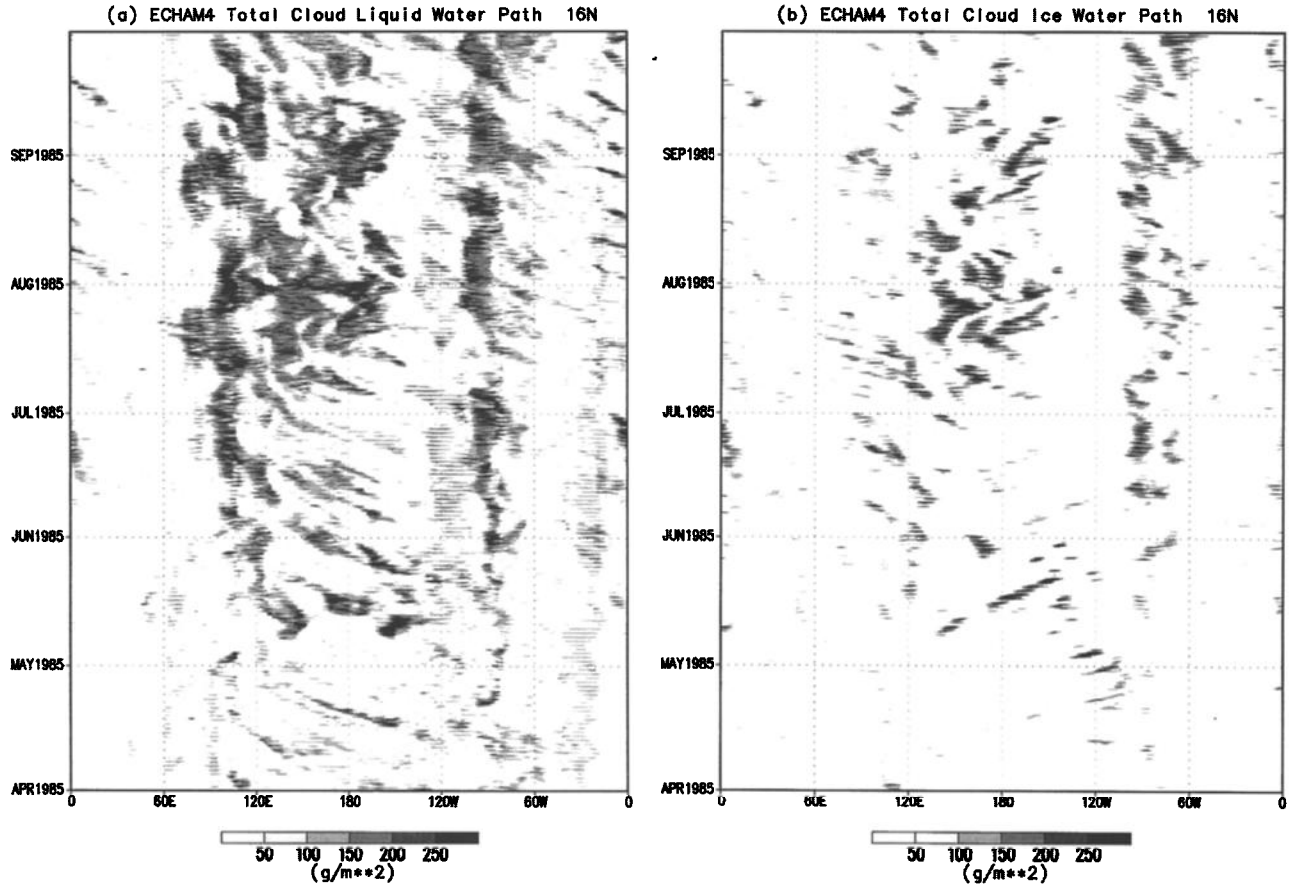

Figure 14. Longitude-time distribution of the (a) total cloud liquid water path and (b) total cloud ice water path as simulated by ECHAM4 at 16.25°N from April to September 1985.

5. Summary

This study documents several cloud parameters simulated by the latest version of the atmospheric GCM (ECHAM4) at the Max Planck Institute for Meteorology and evaluates them by using a variety of observations. Because of the limitation and considerable uncertainties in the cloud-related observations we choose to evaluate only the total cloud amount and total CLWP and reveal further information on simulated cloud microphysical properties (e.g., ice water path and effective drop radii in cloud water). Although some deficiencies remain, the simulated climatological mean and space-time variations of the selected cloud parameters are in reasonable agreement with the available observations.

The global and hemispheric mean of annually and monthly averaged total cloud amount simulated by model differs by less than 5% from satellite or surface-based cloud observations. Although the latitudinal structure of the simulated total cloud amount qualitatively agrees with observations, there is a systematic underestimate in the subtropics and midlatitudes. The phase of the seasonal cycle of simulated total cloud amount is similar to ISCCP equatorward of 40°. Cloud climatology from surface observations has a 1-month lag in comparison with ISCCP and model data in the tropics. Deviating results of the seasonal cycle from the two observations in the higher latitude show the lack of our knowledge of cloud variation over the polar regions. For the diurnal variation, some of the observed trends over land and ocean are reproduced by the model. Regionally, the major discrepancy in the simulated total cloud amount is found over the midlatitude oceans. The systematic underestimate in total cloud amount also leads to the underestimate of the planetary albedo over these regions [*Chen and Roeckner*, 1996]. There are also underestimates in the total cloud amount over the subtropical eastern ocean basins. This discrepancy again can be linked to the problem in simulating the regional radiation budget. The slight difference in the longitudinal structure of total cloud amount in the tropics is related to the simulation of the overall tropical longitudinal circulation. In comparison with the observations, less day-to-day variation in the simulated total cloud amount is found mostly over the tropical convective regions as a result of persistently large daily mean cloud cover found in the model. On the other hand, the persistently large total cloud amounts over the midlatitude oceans in the ISCCP data reveal less day-to-day variation. Lack of interannual variability in the simulation of tropical total cloud amount in comparison with that in the observations is contradictory to the very sensitive interannual variation of the simulated water vapor amount in the tropics [*Chen et al.*, 1996]. These results point to some directions in improving the cloud parameterization.

The satellite retrieval also provides a preliminary attempt to obtain near-global coverage of cloud microphysical properties. Although the observational data still seriously suffer from their large uncertainties, it is an unavoidable first step toward a better product. The rather limited information is still very

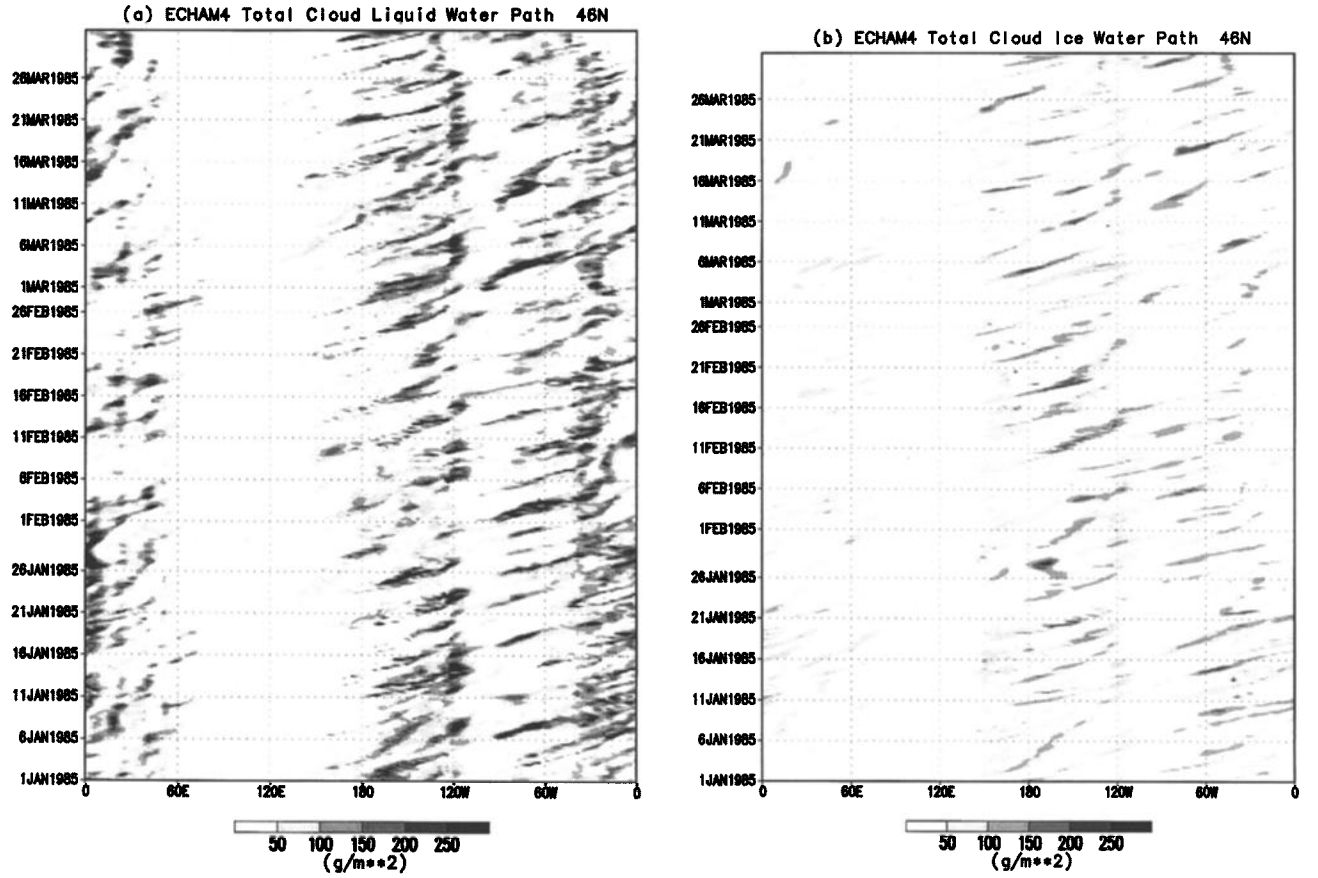

Figure 15. Longitude-time distribution of the (a) total cloud liquid water path and (b) total cloud ice water path as simulated by ECHAM4 at 46.25°N from January to March 1985.

helpful in guiding the equally preliminary study on representing cloud microphysical properties in the climate model (e.g., estimating the reasonable range of parameters, main spatial pattern). Despite large systematic differences among the different data sets, global and hemispheric mean total CLWP in July are larger than in January in all three data sets. However, larger annual mean observed total CLWP in the southern hemisphere than the northern hemisphere is not captured by the model. The latitudinal distribution of the annual mean total CLWP as simulated by the model shows the peak feature in the ITCZ as well as both SSM/I retrievals. While the simulated total CLWP is within the bound revealed in different retrieval methods using SSM/I data at other latitudes, less contrast between the magnitude of total CLWP in the subtropics and midlatitudes is found in the simulation. This finding also provides useful information for further model improvement. The phase of the seasonal cycle in simulated total CLWP agrees reasonably well with the observed phases. However, the amplitude of the seasonal cycle in zonal mean total CLWP is different between the model and the observations and between the two observations. The observed diurnal cycle of total CLWP in the tropics as discussed in the literature is also simulated in the model. Strong tropical interannual variation of total CLWP in the model is a result of circulation changes during the ENSO cycles. Two observational data sets show different degrees extent of sensitivity to the SST anomalies. The main pattern of observed geographic distribution of total CLWP is well simulated, although systematic differences in the summertime midlatitude ocean are found in comparison with one SSM/I retrieval. Another discrepancy in the pattern of simulated total CLWP is the local minimum in the summer subtropical eastern ocean basin, where a local maximum is found in both observational data sets.

Without adequate observational data of ice water path distribution for model validation we show only the model result. It is meant to illustrate a more complete set of the simulated cloud parameters, although the phase partitioning inside the cloud uses a simple empirical function based on cloud temperature. The simulated large-scale circulation in the tropics and the seasonal temperature variation in the higher latitudes show clearly their impacts on the ice water path. Reasonable land-sea contrast of the effective radii of cloud droplets in the tropical lower troposphere is captured by the model, using the simple approach of prescribing different cloud drop number concentrations over continents and oceans, respectively. There are larger differences in comparison with the observations in the midlatitudes. The simple prescription method fails to represent certain physical processes (e.g., advection of air mass and precipitation) indicated in the observations. Further detailed validation of the simulated distribution of cloud parameters requires progress in developing various remote sensing techniques or new instruments to improve our knowledge of the detailed vertical distribution of cloud amount and microphysical properties. The strategy and methodology for model

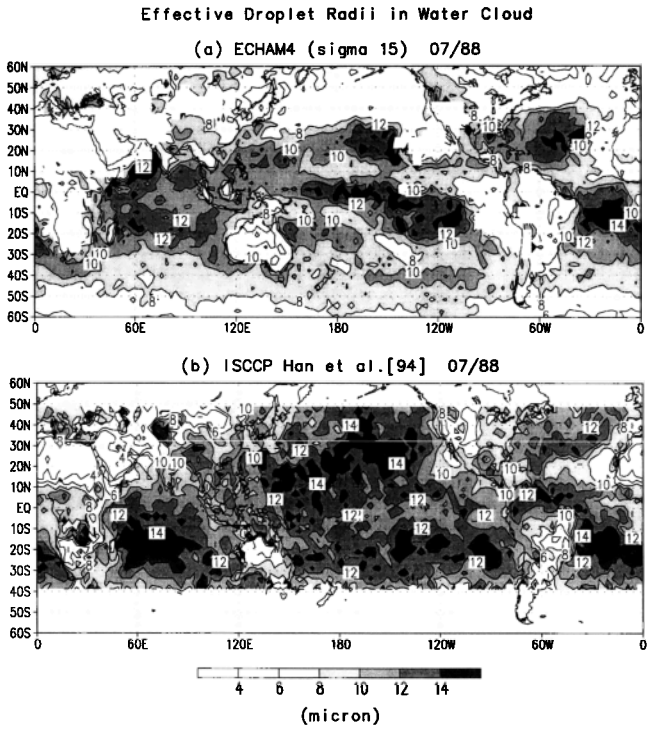

Figure 16. Geographic distribution of the 1988 July mean effective droplet radii in water cloud for (a) hybrid vertical level 15 in ECHAM4 (Sigma 15) and (b) ISCCP [*Han et al.*, 1994].

validation with the available cloud-related observations also deserve further investigation. There is no doubt that not only the mean state, but also the variability of cloud parameters in the model should be carefully examined.

Acknowledgments. We would like to thank Lennart Bengtsson and Ulrike Lohmann for examining a preliminary draft of the manuscript and for offering many invaluable suggestions. We are also grateful to the helpful comments by the anonymous reviewers. The ISCCP datasets are produced through an effort led by W. B. Rossow at the NASA Goddard Institute of Space Studies. The further processed data tapes have been provided to us by Mark W. Crane at the NOAA Geophysical Fluid Dynamics Laboratory. The SSM/I cloud water data are kindly provided by T. Greenwald and F. Weng. We also thanks Q. Han for providing the effective cloud droplet radii data.

References

Albrecht, B. A., Aerosols, cloud microphysics, and fractional cloudiness, *Science*, *245*, 1227–1230, 1989.

Boucher, O., and U. Lohmann, The sulfate-CCN-cloud albedo effect: A sensitivity study with two general circulation models, *Tellus*, *Sect. B47*, 281–300, 1995.

Cess, R. D., et al., Intercomparison and interpretation of climate feedback processes in 19 atmospheric general circulation models, *J. Geophys. Res.*, *95*, 16,601–16,615, 1990.

Charlson, R. J., S. E. Schwartz, J. M. Hale, R. D. Cess, J. A. Coakley Jr., J. E. Hansen, and D. J. Hofmann, Climate forcing by anthropogenic aerosol, *Science*, *255*, 423–430, 1992.

Chen, C.-T., and E. Roeckner, Validation of the Earth radiation budget as simulated by the Max Planck Institute for Meteorology general circulation model ECHAM4 using satellite observations of the Earth Radiation Budget Experiment, *J. Geophys. Res.*, *101*, 4269–4287, 1996.

Chen, C.-T., E. Roeckner, and B. J. Soden, A comparison of satellite observations and model simulations of column integrated moisture and upper tropospheric humidity, *J. Clim.*, *9*, 1561–1585, 1996.

Fowler, L. D., D. A. Randall, and S. A. Rutledge, Liquid and ice cloud microphysics in the CSU general circulation model, I, Model description and simulated microphysical processes, *J. Clim.*, *9*, 489–529, 1996.

Gates, W. L., AMIP: The atmospheric model intercomparison project, *Bull. Am. Meteorol. Soc.*, *73*, 1962–1970, 1992.

Greenwald, T. J., G. L. Stephens, and T. H. Vonder Haar, A physical retrieval of cloud liquid water over the global oceans using special sensor microwave/imager (SSM/I) observation, *J. Geophys. Res.*, *98*, 18,471–18,488, 1993.

Hahn, C. J., S. G. Warren, and J. London, Climatological data for clouds over the globe from surface observations, 1982–1991: The total cloud edition, *Rep. ORNL/CDIAC-72, NDP-026A*, Oak Ridge Natl. Lab., Oak Ridge, Tenn., 1994.

Han, Q., W. B. Rossow, and A. Lacis, Near-global survey of effective droplet radii in liquid water clouds using ISCCP data, *J. Clim.*, *7*, 465–497, 1994.

Heymsfield, A. J., Precipitation development in stratiform ice cloud: A microphysical and dynamical study. *J. Atmos. Sci.*, *34*, 367–381, 1977.

Intergovernmental Panel on Clim. Control, *Climate Change: The Supplementary Report to the IPCC Scientific Assessment*, edited by J. T. Houghton, B. A. Callander, and S. K. Varney, 200 pp., Cambridge Univ. Press, New York, 1992.

Karstens, U., C. Simmer, and E. Ruprecht, Remote sensing of cloud liquid water, *Meteorol. Atmos. Phys.*, *54*, 157–171, 1994.

Kiehl, J. T., Sensitivity of a GCM climate simulation to differences in continental versus maritime cloud drop size, *J. Geophys. Res.*, *99*, 23,107–23,115, 1994.

Lau, N.-C., and M. W. Crane, A satellite view of the synoptic-scale organization of cloud cover in midlatitude and tropical circulation systems, *Mon. Weather Rev.*, *103*, 1984–2006, 1995.

Liou, K. N., and S. C. Ou, The role of cloud microphysical processes in climate: An assessment from one-dimensional perspective, *J. Geophys. Res.*, *94*, 8599–8607, 1989.

Liu, G., and J. A. Curry, Determination of characteristic features of cloud liquid water from satellite microwave measurements, *J. Geophys. Res.*, *98*, 5069–5092, 1993.

Matveev, L. T., *Cloud Dynamics*, 340 pp., D. Reidel, Norwell, Mass., 1984.

McFarlane, N. A., G. J. Boer, J. P. Blanchet, and M. Lazare, The Canadian Climate Centre second-generation general circulation model and its equilibrium climate, *J. Clim.*, *5*, 1013–1044, 1992.

Minnis, P., and E. F. Harrison, Diurnal variability of regional cloud and clear-sky radiative parameters derived from GOES data, II, November 1978 cloud distribution, *J. Clim. Appl. Meteorol.*, *23*, 1012–1031, 1984.

Nordeng, T. E., Extended versions of the convective parameterization scheme at ECMWF and their impact on the mean and transient activity of the model in the tropics, *Tech. Memo. 206*, Res. Dep. Eur. Cent. for Medium Range Weather Forecasts, Reading, England, 1994.

Randall, D. A., J. A. Coakley, C. W. Fairall, R. A. Kropfli, and D. H. Lenschow, Outlook for research on subtropical marine stratiform clouds, *Bull. Am. Meteorol. Soc.*, *65*, 1290–1301, 1984.

Roeckner, E., U. Schlese, J. Biercamp, and P. Loewe, Cloud optical depth feedbacks and climate modelling, *Nature*, *329*, 138–140, 1987.

Roeckner, E., M. Rieland, and E. Keup, Modelling of cloud and radiation in the ECHAM model, *ECMWF/WCRP Workshop on Clouds, Radiative Transfer and the Hydrological Cycle, 12–15 Nov. 1990*, pp. 199–222, Eur. Cent. for Medium-Range Weather Forecasts, Reading, England, 1991.

Roeckner, E., K. Arpe, L. Bengtsson, M. Christoph, M. Claussen, L. Dümenil, M. Esch, M. Giorgetta, U. Schlese, and V. Schulzweida, The atmospheric general circulation model ECHAM4: Model description and simulation of present-day climate, *Rep. 218*, 90 pp., Max Planck Inst. für Meteorol., Hamburg, Germany, 1996.

Rossow, W. B., Clouds, in *Atlas of Satellite Observations Related to Global Change*, edited by R. J. Gurney, J. L. Foster, and C. L. Parkinson, Cambridge Univ. Press, New York, 1993.

Rossow, W. B., and A. A. Lacis, Global, seasonal cloud variation from satellite radiance measurements, II, Cloud properties and radiative effects, *J. Clim.*, *3*, 1204–1253, 1990.

Rossow, W. B., and R. A. Schiffer, ISCCP cloud data products, *Bull. Am. Meteorol. Soc.*, *72*, 2–20, 1991.

Smith, R. N. B., A scheme for predicting layer clouds and their water content in a general circulation model, *Q. J. R. Meteorol. Soc.*, *116*, 435–460, 1990.

Somerville, R. C. J., and L. A. Remer, Cloud optical thickness feedbacks in the CO_2 climate problem, *J. Geophys. Res.*, *89*, 9668–9672, 1984.

Sundquist, H., A parameterization scheme for non-convective condensation including prediction of cloud water content, *Q. J. R. Meteorol. Soc.*, *104*, 677–690, 1978.

Sundquist, H., E. Berge, and J. E. Kristjansson, Condensation and cloud parameterization studies with a mesoscale numerical weather prediction model, *Mon. Weather Rev.*, *117*, 1641–1657, 1989.

Tiedtke, M., A comprehensive mass flux scheme for cumulus parameterization in large scale models, *Mon. Weather Rev.*, *117*, 1779–1800, 1989.

Twomey, S. A., The influence of pollution on the shortwave albedo of cloud, *J. Atmos. Sci.*, *34*, 1149–1152, 1977.

Walcek, C. J., Cloud cover and its relationship to relative humidity during a springtime midlatitude cyclone, *Mon. Weather Rev.*, *122*, 1021–1035, 1994.

Warren, S. G., C. J. Hahn, J. London, R. M. Chervin, and R. L. Jenne, Global distribution of total cloud cover and cloud type amounts over land, *Tech. Note NCAR/TN-273+STR*, 29 pp., 200 maps, Natl. Cent. for Atmos. Res., Boulder, Colo., 1986.

Warren, S. G., C. J. Hahn, J. London, R. M. Chervin, and R. L. Jenne, Global distribution of total cloud cover and cloud type amounts over ocean, *Tech. Note NCAR/TN-317+STR*, 40 pp., 170 maps, Natl. Cent. for Atmos. Res., Boulder, Colo., 1988.

Weare, B. C., I. I. Mokhov, and AMIP project members, Evaluation of total cloudiness and its variability in the Atmospheric Model Intercomparison Project, *J. Clim.*, *8*, 2224–2238, 1995.

Weng, F., and N. C. Grody, Retrieval of cloud liquid water using the special sensor microwave imager (SSM/I), *J. Geophys. Res.*, *99*, 25,535–25,551, 1994.

Williamson, D. L., and P. J. Rasch, Two dimensional semi-Lagrangian transport with shape preserving interpolation, *Mon. Weather Rev.*, *117*, 102–129, 1989.

Wylie, D. P., W. P. Menzel, H. M. Woolf, and K. I. Strabala, Four years of global cirrus cloud statistics using HIRS, *J. Clim.*, *7*, 1972–1986, 1994.

Xu, K. M., and S. K. Krueger, Evaluation of cloudiness parameterization using a cumulus ensemble model, *Mon. Weather Rev.*, *119*, 342–367, 1991.

C.-T. Chen, Department of Earth Sciences, National Taiwan Normal University, No. 88, Section 4, Ting Chou Road, Taipei, 117, Taiwan. (e-mail: chen@cloud.geos.ntnu.edu.tw)

E. Roeckner, Max Planck Institute for Meteorology, 20146 Hamburg, Germany.

(Received May 1, 1996; revised November 26, 1996;
accepted November 26, 1996.)